Driving induced coherent quantum energy transport

Xiufeng Cao,[1] Chen Wang,[2,*] and Dahai He[1,†]
[1]*Department of Physics, Xiamen University, Xiamen 361005, China*
[2]*Department of Physics, Zhejiang Normal University, Jinhua 321004, China*

(Received 7 August 2023; accepted 16 November 2023; published 1 December 2023)

Nonequilibrium energy flows in a driven quantum system coupled to two heat baths are investigated to describe microscopic driven-dissipative processes, based on both a canonical transformation and full counting statistics. The main focus is to understand the interference between the coherent driving and bath induced dissipation. We aim to explore efficient modulation of the quantum energy transport, characterized as transient energy flow, by the Rabi driving and the temperature bias. In particular, steady-state energy flow is divided into three components: temperature bias flow, driving flow, and coherence flow. The driving flow is dominated by the external field driving, and the coherence flow is determined by the interference of two side peaks that are blueshifted and redshifted in Mollow's triplet. The energy flow is mainly contributed by the temperature bias flow at a weak driving limit, and the driving flow is in a strong driving regime. The effects of driving amplitude and temperature bias on the steady-state flow are discussed comprehensively. The results may provide guidance for the efficient control of energy and the information transport in nanodevices driven by an optical field.

DOI: 10.1103/PhysRevB.108.245401

I. INTRODUCTION

The microscopic driven-dissipative processes in a quantum system can be generally modeled by the spin-boson model (SBM) [1,2], which describes the interaction between a quantum two-level system and a bosonic bath. The controllable dynamics of the driven spin-boson model (DSBM) is at the core of vastly distinct state-of-the-art quantum technologies, especially in solid-state implementations of individually addressable two-level systems [3]. The DSBM has been widely studied both in experiment and theory, which is highly related to various physical and chemical processes [4,5]. Recently, great progress has been made in the study of controlled coherent dynamics of qubits in quantum nanodevices, such as superconducting devices based on Josephson tunneling junctions [6,7], optically and electrically controlled qubits in quantum dots [8–12], trapped ions [13,14], and nitrogen vacancy center in diamond [15], while a quantum system composed of two/multiple finite-temperature-biased bosonic baths mediated by a driven qubit, i.e., the nonequilibrium driven spin-boson model (NE-DSBM), has been used to study quantum energy transport [16–18].

Recently, the quantumness and limitations of thermal conductance in small quantum systems have attracted considerable attention via quantum dissipation, which results in the quantized thermal conductance of phonons [19,20] and photons [21]. Furthermore, it has been found that the effect of counter-rotating (CR) terms is significant in diverse topics, such as the quantum Zeno effect [22,23], interference between driving and dissipation [24,25], coherent destruction of tunneling and the Bloch-Siegert shift [26,27], the Rabi model with frequency modulation [28,29], and entanglement evolution [30–32]. Here we consider the effect of CR spin-boson coupling on quantum energy transport in the DSBM.

Technically, the reduced system dynamics of the DSBM has been studied using various numerical and analytical methods, e.g., the time-dependent numerical renormalization group [33,34], the quasiadiabatic propagator path integral [35], stochastic dynamical equations [36–38], hierarchical equations of motion [39], the generalized master equations based on Floquet theory [40–42], the noninteracting blip approximation [43–45], polaron transformation [18,46,47], canonical transformation [48], and the variational Davydov approach [49]. We acknowledge that each method has its own advantages and limitations, depending on the spin-boson coupling strength, the bath temperature, and the bath spectral density distribution. Here we extend the analytical method based on the unitary transformation [24,25] to the NE-DSBM at finite-temperature bias. Our method is suitable for the general bath spectral density function. We will show the energy transport in two Ohmic baths. This analytical method provides a practical utility, which enables us to obtain a deep understanding of the interference in quantum energy transport between coherent driving and bath induced dissipation.

In this paper, we calculate the transient and steady-state flows by applying the canonical transformation and full counting statistics. The Rabi driving amplitude and temperature bias are modulated in the NE-DSBM, respectively. The manipulation of a qubit in the periodically time-dependent driving field is commonly described as $H_S = -\Delta\sigma_x/2 + \Omega\cos(\omega_d t)\sigma_z$, with the coherent tunneling strength Δ, the Rabi driving amplitude Ω, driving frequency ω_d, and Pauli operators σ_x and σ_z. As we know, when $\Omega = 0$, the flow is directed from the high-temperature bath to the low-temperature

*wangchen@zjnu.cn
†dhe@xmu.edu.cn

one, and the steady-state flow vanishes as the two baths' temperatures become equal. We demonstrate that when $\Omega \neq 0$, the transient energy flow presents damped oscillation with the oscillation frequency and the decay rate identical to their counterparts in quantum dissipation dynamics. When the driving amplitude is large, the steady-state flow to the high-temperature bath becomes positive, which means that external driving generates a positive energy flow to the high-temperature baths. By setting low temperatures of two reservoirs, the steady-state flow shows nonmonotonic behavior, which first intensifies dramatically and then slowly decreases with the increase of the Rabi driving amplitude. In particular, the energy flow is divided into three components: temperature bias flow, driving flow, and coherence flow. In particular, the coherence flow is a consequence of the interference between dissipation and driving.

In our Hamiltonian, the interaction of the spin bath and the spin driving are commutative, i.e., both are coupled to σ_z, while the bare spin tunneling $-\Delta\sigma_x/2$ and the external driving $\Omega\cos(\omega_{\rm d}t)\sigma_z$ are noncommutative. Our analysis shows that the driving flow comes from the noncommutativity of the spin tunneling with the external driving and the spin-bath coupling. Moreover, we discuss the steady-state flow with modulations of the temperature bias and various driving amplitudes.

We find that in the weak driving regime, the temperature bias flow and the driving flow are both weakened, resulting in the steady-state flow in the low-temperature area of the right bath that is insensitive to the change in the left bath's temperature. With the increase of Rabi driving, the temperature bias flow and driving flow become strengthened, and the total energy flow gradually changes from being dominated by temperature bias flow to being dominated by driving flow. In the NE-DSBM, the Rabi driving amplitude Ω and the temperature, $T_{\rm L}$ and $T_{\rm R}$, have cooperative effects on the nonequilibrium energy transport, which will yield new applications in two- and three-terminal thermal devices.

This paper is organized as follows: In Sec. II, we introduce the Hamiltonian of the NE-DSBM, and we establish the dynamical equation by using the canonical transformation and full-counting statistics. The transient and steady-state energy flow for various driving Ω, and the temperatures $T_{\rm L}$ and $T_{\rm R}$, are presented and discussed in Sec. III. Finally, the conclusion is given in Sec. IV.

II. MODEL AND THEORY

A. Model

The NE-DSBM consists of one periodically driven spin coupled to two bosonic reservoirs at different temperatures. The schematic diagram is shown in Fig. 1(a). The Hamiltonian is described as ($\hbar = 1$ and $k_B = 1$)

$$\begin{aligned} H &= H_S + H_B + H_I \\ &= -\frac{1}{2}\Delta\sigma_x + \Omega\cos(\omega_{\rm d}t)\sigma_z + \sum_{k,\nu}\omega_{k,\nu}a^\dagger_{k,\nu}a_{k,\nu} \\ &\quad + \sum_{k,\nu}\frac{g_{k,\nu}}{2}(a^\dagger_{k,\nu} + a_{k,\nu})\sigma_z, \end{aligned} \tag{1}$$

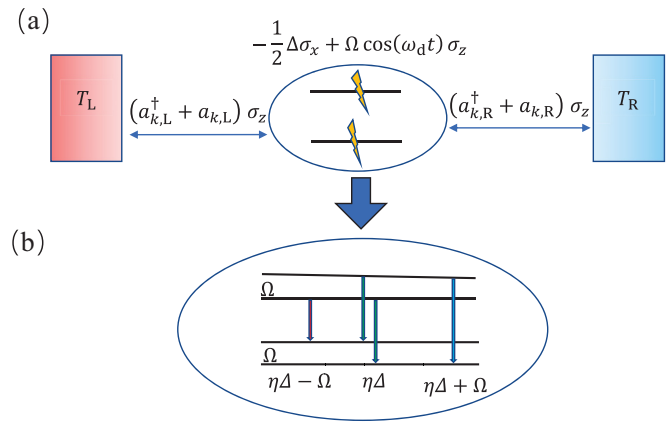

FIG. 1. (a) A schematic diagram of the nonequilibrium driven spin-boson model consisting of a period-driven spin is coupled to two finite-temperature boson baths. The driving and dissipation couple to σ_z. (b) The transitions are depicted, and the corresponding frequencies of the phonon are $\eta\,\Delta$, $\eta\,\Delta - \Omega$, and $\eta\,\Delta + \Omega$. We see that the transition strength of phonons with unshifted frequencies ($\eta\,\Delta$) is twice that of the two types of phonons with side-shifted frequencies ($\eta\,\Delta - \Omega$ and $\eta\,\Delta + \Omega$).

where σ_z and σ_x are the Pauli matrices, and Δ is the coherence tunneling of the spin. The operator $a^\dagger_{k,\nu}$ ($a_{k,\nu}$) creates (annihilates) one boson with the frequency $\omega_{k,\nu}$ in the ν bath for $\nu = ({\rm L}, {\rm R})$. The parameter $g_{k,\nu}$ shows the coupling strength between the spin and the ν bath. The driving and dissipation are coupled to σ_z and commutative to each other. But the tunneling of the spin is in the σ_x-direction, and is noncommutative with dissipation and driving. Therefore, in this paper we discuss the interference of driving and dissipating in the same direction on energy transfer, whether they reinforce or weaken each other. Here, the coupling of the spin and the ν bath is characterized by the spectral function as $G_\nu(\omega) = \sum_{k,\nu} g^2_{k,\nu}\delta(\omega - \omega_k) = 2\alpha_\nu\omega^s\omega_{c,\nu}^{1-s}\theta(\omega_{c,\nu} - \omega)$, where α_ν is the dimensionless spin-bath coupling strength, $\omega_{c,\nu}$ is the cutoff frequency of the ν bath, and $\theta(x)$ is the usual step function. In this work, we specify the Ohmic spectrum $s = 1$ to characterize the reservoirs and select the system-reservoir interaction strength away from the quantum criticality.

We mainly study the response of the energy flow to the external driving field. With the Rabi frequency Ω increasing from small to large, the energy spectrum of spin changes from a single peak to a Mollow triplet, i.e., the tunneling energy changes from Δ to $\eta\Delta$ and $\eta\Delta \pm \Omega$, as shown in Fig. 1(b), where η is the renormalized coefficient from the polaronic qubit-bath interaction, which will be discussed later. Here we choose the parameter $\Omega \leqslant \Delta$, which is different from the strong driving case ($\Omega \gg \Delta$) in Refs. [41,42]. In the strong driving, when the ratio of driving amplitude to driving frequency is the root of the Bessel function, the coherent destruction of tunneling (CDT) occurs, which freezes the qubit dynamics. In this paper, our parameter condition is set as $\Omega \leqslant \Delta$, where there is no CDT effect.

In the following, we generalize the Hamiltonian by including the auxiliary counting field χ. When setting $\chi = 0$, the conventional Hamiltonian is recovered. The full counting statistics (FCS) as a mathematically rigorous

method is usually applied to measure the arbitrary order of the energy current fluctuation [50], of which the lowest order gives the energy flow. To count the energy transported in, e.g., the right bath, we add the counting term to the whole Hamiltonian [45,51] as $H_\chi = H_S + H_B + H_I(\chi) = \exp(i\chi \sum_k \omega_{k,\mathrm{R}} a^\dagger_{k,\mathrm{R}} a_{k,\mathrm{R}}/2) H \exp(-i\chi \sum_k \omega_{k,\mathrm{R}} a^\dagger_{k,\mathrm{R}} a_{k,\mathrm{R}}/2)$, where the χ-dependent interaction Hamiltonian is obtained as

$$H_I(\chi) = \sum_k \frac{g_{k,\mathrm{R}}}{2}[a^\dagger_{k,\mathrm{R}} e^{\frac{i\chi}{2}\omega_{k,\mathrm{R}}} + a_{k,\mathrm{R}} e^{-\frac{i\chi}{2}\omega_{k,\mathrm{R}}}]\sigma_z + \sum_k \frac{g_{k,\mathrm{L}}}{2}(a^\dagger_{k,\mathrm{L}} + a_{k,\mathrm{L}})\sigma_z. \tag{2}$$

Taking into account CR correlation of the spin and baths, we apply the canonical transformation [48,52,53], $H' = \exp(S_{\mathrm{R+L}}) H_\chi \exp(-S_{\mathrm{R+L}})$, with the generator $S_{\mathrm{R+L}} = S_\mathrm{R} + S_\mathrm{L}$. And S_ν is given as $S_\nu = \sum_k \frac{g_{k,\nu}\xi_{k,\nu}}{2\omega_{k,\nu}}[a^\dagger_{k,\nu} e^{\frac{i\chi\delta_{\nu,\mathrm{R}}\omega_{k,\nu}}{2}} - a_{k,\nu} e^{-\frac{i\chi\delta_{\nu,\mathrm{R}}\omega_{k,\nu}}{2}}]\sigma_z$, and the renormalization parameter $\xi_{k,\nu} = \omega_{k,\nu}/(\omega_{k,\nu} + \eta_\nu \Delta)$. Up to the order of $g_{k,\nu}$, the transformed Hamiltonian H' is written as $H' = H'_0 + H'_1$, where the renormalized spin and first-order spin-bath interaction terms are given by

$$H'_0 = \frac{1}{2}\eta\,\Delta\,s_z + \Omega\cos(\omega_\mathrm{d} t)(s_+ + s_-) + \sum_{k,\nu}\omega_{k,\nu} a^\dagger_{k,\nu} a_{k,\nu} - \sum_{k,\nu}\frac{|g_{k,\nu}|^2}{4\omega_{k,\nu}}\xi_{k,\nu}(2 - \xi_{k,\nu}) \tag{3}$$

and

$$H'_1(\chi) = \sum_k \tilde{g}_{k,\mathrm{R}}\left(a^\dagger_{k,\mathrm{R}} s_- e^{\frac{i\chi\omega_{k,R}}{2}} + a_{k,\mathrm{R}} s_+ e^{-\frac{i\chi\omega_{k,R}}{2}}\right) + \sum_k \tilde{g}_{k,\mathrm{L}}(a^\dagger_{k,\mathrm{L}} s_- + a_{k,\mathrm{L}} s_+), \tag{4}$$

respectively, with $\eta = \eta_\mathrm{R}\,\eta_\mathrm{L}$. Here we define the renormalized spin tunneling as $\eta\,\Delta$, the spin-bath interaction parameter $\tilde{g}_{k,\nu} = (\frac{\eta_\nu \Delta}{\omega_{k,\nu} + \eta_\nu \Delta})g_{k,\nu}$, and

$$\eta_\nu = \exp\left[-\sum_k \frac{g^2_{k,\nu}}{2\omega^2_{k,\nu}}\,\xi^2_{k,\nu}\coth\left(\frac{\omega_{k,\nu}}{2T_\nu}\right)\right]. \tag{5}$$

The creation and annihilation operators are denoted as $s_z = |s_1\rangle\langle s_1| - |s_2\rangle\langle s_2|$, $s_+ = |s_2\rangle\langle s_1|$ and $s_- = |s_1\rangle\langle s_2|$, in which the states $|s_1\rangle$ and $|s_2\rangle$ are the corresponding eigenstates of σ_x, written as $\sigma_x|s_{1(2)}\rangle = +(-)|s_{1(2)}\rangle$.

In the definition of η_ν, if the temperature of two baths is different ($T_\mathrm{L} \neq T_\mathrm{R}$), η_L is not equal to η_R. Therefore, the coupling strength of renormalization $\tilde{g}_{k,\nu}$ is dependent on η_ν. Hence, even if the dimensionless spin-bath coupling strengths of two baths are the same ($\alpha_\mathrm{L} = \alpha_\mathrm{R}$), the effective coupling strengths after canonical transformation of the two baths ($\tilde{g}_{k,\mathrm{L}}$ and $\tilde{g}_{k,\mathrm{R}}$) are different when the temperatures of the two baths are different, i.e., asymmetric caused by temperature.

In the following, we solve the equation of motion of the density matrix in the rotating frame with the rotating operator $R(t) = \exp[-\frac{i}{2}\omega_\mathrm{d}(s_z + \sum_{k,\nu} a^\dagger_{k,\nu} a_{k,\nu})t]$, and the Hamiltonian becomes

$$H'(\chi) = \frac{1}{2}(\eta\,\Delta - \omega_\mathrm{d})\,s_z + \frac{1}{2}\Omega(s_+ + s_-) + \sum_{k,\nu}(\omega_{k,\nu} - \omega_\mathrm{d})a^\dagger_{k,\nu} a_{k,\nu} + \sum_k \tilde{g}_{k,\mathrm{R}}\left(a^\dagger_{k,R} s_- e^{\frac{i\chi\omega_{k,\mathrm{R}}}{2}} + a_{k,R} s_+ e^{-\frac{i\chi\omega_{k,\mathrm{R}}}{2}}\right) + \sum_k \tilde{g}_{k,\mathrm{L}}(a^\dagger_{k,\mathrm{L}} s_- + a_{k,\mathrm{L}} s_+), \tag{6}$$

where the two high-frequency terms $e^{\pm i2\omega_\mathrm{d}}$ related to the counter-rotating terms of the qubit driving are approximately ignored.

Generally, one may bound the validity of the rotating-wave approximation (RWA) of the qubit driving by the safe scope $\Omega \ll \Delta$. It is also known that the increase of the driving amplitude Ω with counter-rotating terms is expected to modify the behaviors of the currents with RWA. Though not shown here, by including the influence of counter-rotating terms with the Floquet master equation [4], we find that both the transient and steady-state currents provided by the RWA and the Floquet master equation are qualitatively the same in the regime of $\Omega \leqslant \Delta$, with certain quantitative deviations. Hence, we believe that the RWA of qubit driving can be approximately adopted as $\Omega \leqslant \Delta$, which enables us to obtain the analytical expression of the currents in the following.

Now the static Hamiltonian $H'(\chi)$ (6) has the same form as the Hamiltonian in the RWA. But the parameters are renormalized to include the effects of the CR terms ($a^\dagger_{k,\mathrm{R}} s_+$ and $a_{k,\mathrm{R}} s_-$). The energy detuning between the driving amplitude and the energy level of spin is $\omega_\mathrm{d} - \eta\,\Delta$. We consider the resonant case $\omega_\mathrm{d} = \eta\,\Delta$ in this paper, and the energy flow under the nonresonant condition can be straightforwardly extended in future study.

B. Equation of motion of the density matrix

We derive the master equation of the NE-DSBM combined with the FCS, and the equation of motion of the density matrix ρ_{SB} for the spin (S) and bath (B) is given by $d\rho_{SB}(t)/dt = -i[H, \rho_{SB}(t)]$. After unitary transformations, we have the equation of motion $d\rho'_{SB}(\chi, t)/dt = -i[H'(\chi), \rho'_{SB}(\chi, t)]_\chi$, where $[A(\chi), B(\chi, t)]_\chi = A(\chi)B(\chi, t) - B(\chi, t)A(-\chi)$, and $\rho'_{SB} = \exp(S_{\mathrm{R+L}})\rho_{SB}\exp(-S_{\mathrm{R+L}})$ is the density matrix in the Schrödinger picture with the transformed Hamiltonian $H'(\chi)$. The details of the derivation of the equation of motion are in Appendix A.

Using the Kronecker product property and the technique of the Lyapunov matrix equation, we expand the density matrix into a vector, $|\rho'_S(\chi, t)\rangle = |\rho'_{11}(\chi, t), \rho'_{12}(\chi, t), \rho'_{21}(\chi, t), \rho'_{22}(\chi, t)\rangle$. Here the subscript of ρ_S (1 and 2) indicates the eigenstates of σ_x, $|s_1\rangle$ and $|s_2\rangle$, thus $\rho'_S(\chi, t)$ is the density matrix in the eigenspace of σ_x. The equation of motion is expressed as

$$\frac{d}{dt}\rho'_S(\chi, t) = \hat{\mathcal{L}}(\chi)|\rho'_S(\chi, t)\rangle, \tag{7}$$

where $\hat{\mathcal{L}}(\chi)$ is the Liouvillian superoperator. Generally, the reduced density matrix is given by $|\rho'_S(\chi,t)\rangle = \exp[\hat{\mathcal{L}}(\chi)t]|\rho'_S(\chi,0)\rangle$, where $|\rho'_S(\chi,0)\rangle$ is the initial state, which is specified in this work as $|\rho'_S(\chi,0)\rangle = [1,1,1,1]^{\mathrm{T}}/2$. Therefore, the cumulant-generating function is obtained, $F_t(\chi) = \partial \ln \mathcal{Z}_\chi(t)/\partial t$, with the cumulant function $\mathcal{Z}_\chi(t) = \mathrm{Tr}_S[\rho'_S(\chi,t)]$. In the rotating frame, the Hamiltonian (6) and the superoperator $\hat{\mathcal{L}}(\chi)$ are time-independent, and $\rho'_S(t)$ has a steady-state solution. Then the corresponding nth cumulant of energy current fluctuations is given by $J^{(n)}(t) = \partial^n F_t(\chi)/\partial(i\chi)^n|_{\chi=0}$. In particular, the energy flux is the first cumulant $J(t) = \partial F_t(\chi)/\partial(i\chi)|_{\chi=0}$. Equation (7) is solved with the Laplace transformation in Appendix B, and we obtain the regrouped density matrix $|\rho''_S(\chi,t)\rangle = |\rho''_{11}(\chi,t), \rho''_{12}(\chi,t), \rho''_{21}(\chi,t), \rho''_{22}(\chi,t)\rangle$ with $\rho''_{11}(\chi,t) = \rho'_{11}(\chi,t) - \rho'_{22}(\chi,t)$, $\rho''_{12}(\chi,t) = \rho'_{21}(\chi,t) - \rho'_{12}(\chi,t)$, $\rho''_{21}(\chi,t) = \rho'_{21}(\chi,t) + \rho'_{12}(\chi,t)$, and $\rho''_{22}(\chi,t) = \rho'_{11}(\chi,t) + \rho'_{22}(\chi,t)$. Then, the cumulant function is expressed as $\mathcal{Z}_\chi(t) = \langle I|\rho''_S(\chi,t)\rangle$, with the vector defined as $\langle I| = \langle 0,0,0,1|$. The transient flow is

$$J(t) = \frac{\partial L_{41}(\chi)}{\partial(i\chi)}\bigg|_{\chi=0}[\rho'_{11}(t) - \rho'_{22}(t)] + \frac{\partial L_{43}(\chi)}{\partial(i\chi)}\bigg|_{\chi=0}[\rho'_{12}(t) + \rho'_{21}(t)] + \frac{\partial L_{44}(\chi)}{\partial(i\chi)}\bigg|_{\chi=0}. \tag{8}$$

In the eigenspace of σ_x, the diagonal and off-diagonal terms of the density matrix correspond to $\langle\sigma'_x(t)\rangle = \rho'_{11}(t) - \rho'_{22}(t)$ and $\langle\sigma'_z(t)\rangle = \rho'_{21}(t) + \rho'_{12}(t)$, which correspond to the nonequilibrium correlation in the Hamiltonian (6) with $\chi = 0$. In Eq. (8), the first and second terms give the time-dependent evolution part of $J(t)$ related to the dynamics of $\rho'_{11}(t) - \rho'_{22}(t)$ and $\rho'_{21}(t) + \rho'_{12}(t)$. The third term is a constant independent of time. The transient flow, Eq. (8), is one of the main results of our paper and gives the relationship between the energy flow and the dynamic quantities of the nonequilibrium spin-boson model. Also, Eq. (8) can be naturally reduced to the previous result [48] in the absence of an external driving field.

C. Steady-state energy flow

We study the expression of the steady-state energy flow in FCS. We count the energy flow in the right bath. Then, we derive the steady-state flow at the long-time limit in Appendix C, which is expressed as

$$J_{\mathrm{ss}} \equiv J(t\to\infty) = \frac{\partial L_{41}(\chi)}{\partial(i\chi)}\bigg|_{\chi=0}(\rho'_{11} - \rho'_{22})_{\mathrm{ss}} + \frac{\partial L_{43}(\chi)}{\partial(i\chi)}\bigg|_{\chi=0}(\rho'_{12} + \rho'_{21})_{\mathrm{ss}} + \frac{\partial L_{44}(\chi)}{\partial(i\chi)}\bigg|_{\chi=0}, \tag{9}$$

where the first derivative of the counting-field embedded Liouvillian operator elements is obtained in Eqs. (C4a)–(C4c). In the resonant case, the steady-state dynamics of density matrix elements can be analytically solved as

$$(\rho'_{11} - \rho'_{22})_{\mathrm{ss}} = \frac{\gamma_-\Gamma_-\Gamma_1 - \gamma\Gamma_+\Gamma_1}{\Gamma_+(\Gamma\Gamma_1 + 2\Omega^2)}, \tag{10a}$$

$$(\rho'_{12} + \rho'_{21})_{\mathrm{ss}} = \frac{\gamma_-}{\Gamma_+}, \tag{10b}$$

where the combined spectral function denotes $\gamma_- = \sum_{\nu=(\mathrm{R,L})}[\gamma_\nu(\eta\,\Delta - \Omega) - \gamma_\nu(\eta\,\Delta + \Omega)]$ and the combined transition rates are $\Gamma_\pm = \sum_{\nu=(\mathrm{R,L})}(\Gamma_{\nu,2} \pm \Gamma_{\nu,3})$, $\Gamma_1 = \sum_{\nu=(\mathrm{R,L})}\Gamma_{\nu,1}$, and $\Gamma = 2\Gamma_1 + \Gamma_+$, with the rate $\Gamma_{\nu,j} = [1 + 2n_\nu(\omega_j)]\gamma_{\nu,j}$, the Bose-Einstein distribution function $n_\nu(\omega_j) = 1/[\exp(\omega_j/k_{\mathrm{B}}T_\nu) - 1]$, and the modified spectral function $\gamma_{\nu,j} = \pi(\eta_\nu\Delta/(\eta\Delta + \omega_j))^2 G_\nu(\omega_j)$, where $j = 1$, 2, and 3 corresponds to the Mollow frequencies $\omega_1 = \eta\Delta$, $\omega_2 = \eta\Delta - \Omega$, and $\omega_3 = \eta\Delta + \Omega$. The results are consistent with previous work [24,25].

The steady-state population bias $(\rho'_{11} - \rho'_{22})_{\mathrm{ss}}$ has two competing terms, which both reflect the cooperative effect of the driving and dissipation, which are characterized by the interference of two side peaks ($\eta\Delta - \Omega$ and $\eta\Delta + \Omega$) of both baths, while the off-diagonal term $(\rho'_{12} + \rho'_{21})_{\mathrm{ss}}$ includes the coefficient γ_-, which also stems from the interference of the Mollow side peaks.

Then, steady-state flow is divides into three components $J_{\mathrm{ss}} = J_{\mathrm{t}} + J_{\mathrm{d}} + J_{\mathrm{c}}$, which are specified as

$$J_{\mathrm{t}} = \omega_1\gamma_{\mathrm{R},1}\Gamma_{\mathrm{e}}\sum_{\substack{j=(1,2,3)\\ \nu=(\mathrm{L,R})}}[(1+\delta_{j,1})\gamma_{\nu,j}(\mathrm{n}_{\nu,j} - \mathrm{n}_{\mathrm{R},1})] + \omega_2\gamma_{\mathrm{R},2}\Gamma_{\mathrm{e}}\sum_{\substack{j=(1,2,3)\\ \nu=(\mathrm{L,R})}}[(1+\delta_{j,1})\gamma_{\nu,j}(\mathrm{n}_{\nu,j} - \mathrm{n}_{\mathrm{R},2})] + \omega_3\gamma_{\mathrm{R},3}\Gamma_{\mathrm{e}}\sum_{\substack{j=(1,2,3)\\ \nu=(\mathrm{L,R})}}[(1+\delta_{j,1})\gamma_{\nu,j}(\mathrm{n}_{\nu,j} - \mathrm{n}_{\mathrm{R},3})], \tag{11a}$$

$$J_{\mathrm{d}} = \frac{\Omega^2}{2(\Gamma\Gamma_1 + 2\Omega^2)}(2\omega_1\gamma_{\mathrm{R},1} + \omega_2\gamma_{\mathrm{R},2} + \omega_3\gamma_{\mathrm{R},3}), \tag{11b}$$

$$J_{\mathrm{c}} = \frac{\gamma_-}{4\Gamma_+}\left[\frac{\Gamma_-\Gamma_1}{\Gamma\Gamma_1 + 2\Omega^2}(2\omega_1\Gamma_{\mathrm{R},1} + \omega_2\Gamma_{\mathrm{R},2} + \omega_3\Gamma_{\mathrm{R},3}) + (\omega_3\Gamma_{\mathrm{R},3} - \omega_2\Gamma_{\mathrm{R},2})\right], \tag{11c}$$

with the Kronecker symbol $\delta_{m,1}$ and the coefficient $\Gamma_{\mathrm{e}} = 2\Gamma_1/(\Gamma\Gamma_1 + 2\Omega^2)$. The flow J_{t} is clearly characterized as three frequencies of the Mollow triplet [54]: $\omega_1 = \eta\,\Delta$, $\omega_2 = (\eta\,\Delta - \Omega)$, and $\omega_3 = (\eta\,\Delta + \Omega)$. Accordingly, J_{t} transfers energy with unshifted frequency $\eta\,\Delta$, redshifted frequency $(\eta\,\Delta - \Omega)$, and blueshifted frequency $(\eta\,\Delta + \Omega)$, respectively, and the transition channels of the unshifted frequency ω_1 are twice that of two side frequencies ω_2 and ω_3, as shown in Fig. 1(b).

The first flow component J_{t} in Eq. (11a) is driven by the bosonic distribution difference $(\mathrm{n}_{\mathrm{L},j} - \mathrm{n}_{\mathrm{R},i})$ and $(\mathrm{n}_{\mathrm{R},j} - \mathrm{n}_{\mathrm{R},i})$. In the absence of external driving ($\Omega = 0$), it is naturally

reduced to the previous result [55]

$$J_{\rm t} = \frac{2(n_{\rm L,1} - n_{\rm R,1})\gamma_{\rm R,1}\gamma_{\rm L,1}\omega_1}{(1+2n_{\rm L,1})\gamma_{\rm L,1} + (1+2n_{\rm R,1})\gamma_{\rm R,1}}. \tag{12}$$

Therefore, it is referred to as the traditional temperature bias flow.

The second flow component $J_{\rm d}$ in Eq. (11b) is explicitly proportional to the square of the driving amplitude, and it is termed the driving flow. The first factor $\Omega^2/2(\Gamma\Gamma_1 + 2\Omega^2)$ comes from the population bias $(\rho'_{11} - \rho'_{22})_{\rm ss}$ and is symmetric about the temperatures of two bosonic baths. The other factor $(2\omega_1\gamma_{R,1} + \omega_2\gamma_{R,2} + \omega_3\gamma_{R,3})$ contains the renormalized spectral function $\gamma_{{\rm R},j} = \pi(\frac{\eta_{\rm R}\,\Delta}{\eta_{\rm R}\,\Delta+\omega_j})^2 G_{\rm R}(\omega_j)$, which becomes asymmetric induced by the temperature of the right bath. This asymmetry becomes significant as the temperature increases, while in the rotating-wave approximation, $\gamma_{{\rm R},j-{\rm RWA}} = \pi G_{\rm R}(\omega_j)/4$ becomes temperature-independent. Then $J_{\rm d-RWA}$ is strictly symmetric about the temperature of the left and right baths. Therefore, the CR terms contribute to the asymmetric behavior of the driving flow component. Even under the weak spin-boson interaction $\alpha_{\rm R} = 0.01$ (corresponding to the renormalized $\eta_{\rm R}$ in the range of 0.90–0.99), the flow component shows obvious asymmetry with the temperature of the two baths.

The third flow component $J_{\rm c}$ in Eq. (11c) is partially contributed by the the steady-state off-diagonal elements $(\rho'_{12} + \rho'_{21})_{\rm ss}$, which stem from the interference of the driving and dissipation. Then $J_{\rm c}$ is termed the coherence flow. From $\gamma_- = \sum_{v=({\rm R,L})}[\gamma_v(\eta\,\Delta - \Omega) - \gamma_v(\eta\,\Delta + \Omega)]$ with $\gamma_{\rm R}(\eta\,\Delta - \Omega) - \gamma_{\rm R}(\eta\,\Delta + \Omega) = 2\pi\alpha_{\rm R}[(\frac{\eta_{\rm R}\,\Delta}{2\eta_{\rm R}\,\Delta-\Omega})^2(\eta\,\Delta - \Omega) - (\frac{\eta_{\rm R}\,\Delta}{2\eta_{\rm R}\,\Delta+\Omega})^2(\eta\,\Delta + \Omega)]$, we find that γ_- is proportional to the first order of the spin-bath coupling strength α in the Ohmic bath. When the driving amplitude $\Omega = 0$, the coherence flow disappears, while in the rotating wave approximation, $\gamma_{-,{\rm RWA}} = -2\pi\alpha\Omega$, and the corresponding coherence flow $J_{\rm c-RWA}$ is always linearly proportional to Ω. This clearly demonstrates the important role of the CR terms on the coherent behaviors (e.g., coherence flow) of the driven-dissipative systems, which is analogous to what was observed in Ref. [56] by applying the stochastic Liouville–von Neumann exact equation to study the Brownian motion. Therefore, it is clear that the CR terms contribute to the nonlinearity behavior of the coherent flow component by tuning Ω. Only in the condition of low temperatures and weak driving is it found that $\gamma_- \approx \gamma_{-{\rm RWA}}$, where the coherence flow is reduced to being proportional to the Rabi frequency Ω. Considering that the driving flow is squarely proportional to Ω, the coherence flow is expected to show behavior that is distinct from the driving flow.

III. RESULTS AND DISCUSSIONS

In this section, we show the transient flow $J(t)$ and steady-state flow $J_{\rm ss}$ of the NE-DSBM, and we discuss the interference effect of the driving and dissipation on energy flows. We set $\Delta = 1$ as the unit. For simplicity, we set the spin-bath coupling strength $\alpha_{\rm L} = \alpha_{\rm R} = 0.01$ and the energy $\eta\,\Delta$ resonant with the driving frequency $\omega_{\rm d} = \eta\,\Delta$, the cutoff frequency $\omega_c = 10$, and the time in the unit of Δ^{-1}. The temperature bias is defined as $\delta T = T_{\rm L} - T_{\rm R}$.

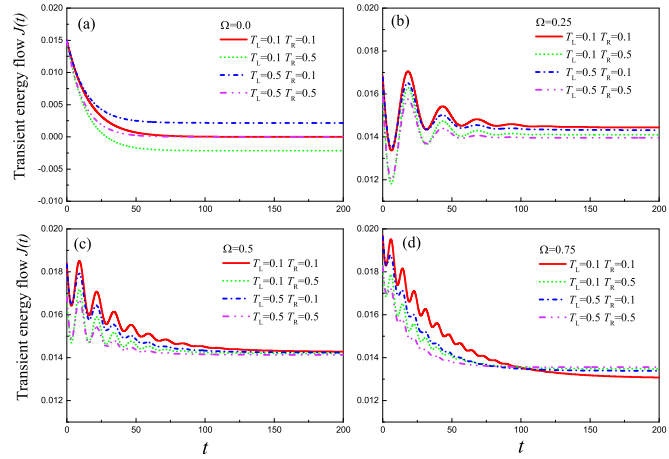

FIG. 2. The transient energy current $J(t)$ for different Rabi driving amplitudes (a) $\Omega = 0.0$, (b) $\Omega = 0.25$, (c) $\Omega = 0.5$, and (d) $\Omega = 0.75$.

In Fig. 2 we plot the transient flow $J(t)$ into the right bath with various external driving Rabi amplitudes $\Omega = 0$, 0.25, 0.5, and 0.75. Specifically, Fig. 2(a) shows the flow in the absence of the driving, where the flow asymptotically tends to the traditional steady-state counterpart. If the temperature bias of the two baths is zero (e.g., $T_{\rm L} = T_{\rm R} = 0.1$), the steady-state flow is expected to be zero. Then, we tune on the driving amplitude to analyze the transient flow in Figs. 2(b)–2(d). When the driving amplitude is not zero, the flow generally exhibits damped oscillation, i.e., the amplitude of oscillation decreases with time and finally reaches the steady-state current. Moreover, the finite steady-state flow is generated even against the temperature bias.

Figure 3 shows the steady-state flow $J_{\rm ss}$ as a function of the driving Rabi frequency Ω. In Fig. 3(a), when $T_{\rm L}$ and $T_{\rm R}$ are low temperature, the steady-state flow first increases rapidly and then decreases slowly by increasing Ω. When the temperature bias is negative (e.g., $T_{\rm L} = 0.1$ and $T_{\rm R} = 0.5$), the negative-to-positive crossover of the steady-state flow can be easily realized by slightly increasing the driving amplitude. Figure 3(b) shows the steady-state flow in the high-temperature region. It is shown that the flow increases obviously with the increase of the Rabi frequency Ω as $\delta T \geqslant 0$, while in the case $\delta T < 0$ (e.g., $T_{\rm L} = 1$ and $T_{\rm R} = 5$), the

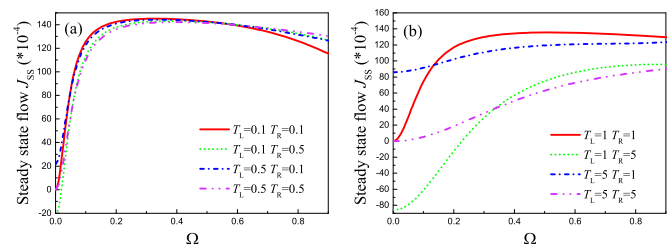

FIG. 3. The steady-state energy current with Rabi frequency Ω. The low-temperature and high-temperature cases are shown in (a) and (b), respectively.

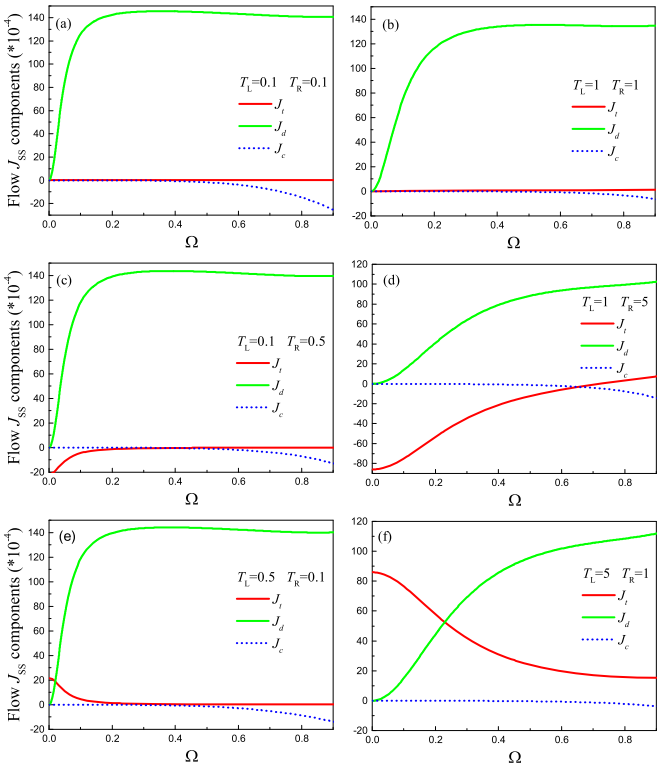

FIG. 4. The three components J_t, J_d, and J_c of the steady-state flow with Rabi frequency Ω. The low-temperature and high-temperature cases are shown in (a), (c), (e) and (b), (d), (f), respectively.

flow changes sign from negative to positive when the Rabi frequency Ω becomes finite (e.g., $\Omega \approx 0.24$). Therefore, we conclude that the additional driving and coherent flows should be considered to analyze quantum energy transport beyond the weak external driving regime.

To give an explicit picture of three flow components (J_t, J_d, and J_c), we plot Fig. 4 by tuning the Rabi frequency Ω. It is interesting to find that the driving flow generally shows dramatic positive enhancement by slightly increasing the driving amplitude Ω, and the coherence flow is negatively enhanced at finite Ω, regardless of the temperature bias. Moreover, in the absence of the temperature bias ($\delta T = 0$) in Figs. 4(a) and 4(b), it is found that the temperature bias flow J_t always becomes vanishing. Hence, the driving and coherence flows dominate energy transport at zero-temperature bias, while at finite temperature bias in Figs. 4(c)–4(f), the temperature bias flow is expected to mainly contribute to the steady-state flow with weak driving amplitude (e.g., $\Omega = 0.02$). By increasing Ω, the temperature bias flow asymptotically approaches zero from the positive value at $\delta T > 0$ and the negative one at $\delta T < 0$. Therefore, it is natural to observe the negative-to-positive crossover of the heat flow in the bias regime of $\delta T < 0$ [e.g., in Fig. 3(b)], considering the competition between the driving flow and the temperature bias flow in Figs. 4(c) and 4(d).

Figure 5 shows the contour plot of steady-state energy flow into the right bath and its components with weak Rabi driving amplitude $\Omega = 0.1$, i.e., the total steady-state flow

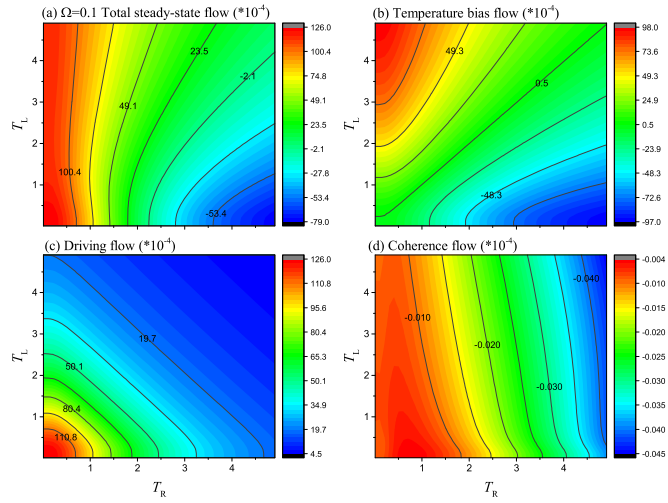

FIG. 5. The contour plot of steady-state flow in weak driving amplitude $\Omega = 0.1$. (a) The total of steady-state flow J_{ss}, (b) temperature bias flow J_t, (c) the driving flow J_d, and (d) the coherence flow J_c.

J_{ss}, temperature bias flow J_t, the driving flow J_d, and the coherence flow J_c. In Fig. 5(a) with $T_R < 1$, the steady-state flow is dramatically affected by the temperature of the right bath. Specifically in Fig. 5(b), the behavior of J_t with the weak driving is analogous to its counterpart in the absence of external driving [48]. The steady-state driving flow J_d in Fig. 5(c) is almost symmetric by tuning the temperature bias. The coherence flow J_c in Fig. 5(d) is almost independent of the temperature of the left bath, and it is negative and small compared to J_t and J_d. Hence, the contribution from J_c to J_{ss} could be ignored in the weak driving case.

Figure 6 plots the contours with the strong driving amplitude $\Omega = 0.8$. The total energy flow in Fig. 6(a) is apparently amplified compared to its weak driving counterpart, which is mainly contributed by the driving flow in Fig. 6(c). This demonstrates the importance of the driving flow in the strong driving regime. In Fig. 6(b), the magnitude of temperature bias

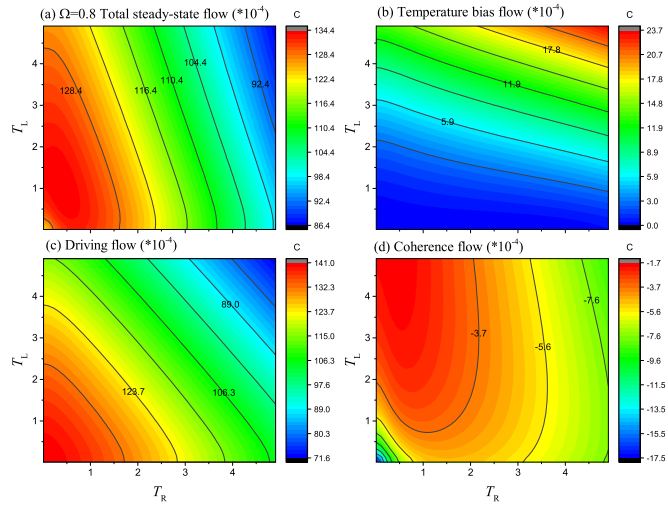

FIG. 6. The same contour plot as Fig. 5 in the driving amplitude $\Omega = 0.8$.

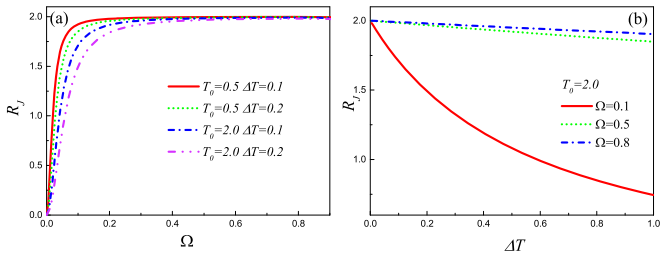

FIG. 7. The effective asymmetric factor of heat current into the Rth reservoir by tuning (a) the driving amplitude and (b) temperature bias, with $T_{\rm L} = T_0 + \Delta T$ and $T_{\rm R} = T_0 - \Delta T$.

flow $J_{\rm t}$ becomes asymmetric and suppressed, in contrast with the weak driving case in Fig. 5(b). For the coherence flow $J_{\rm c}$ in Fig. 6(d), it remains negative and sharply increases by an order of magnitude 10^2 compared with the weak driving case, and it should not be naively ignored by comparing with the temperature bias flow.

Moreover, by observing Figs. 5(a) and 6(a), we find that the flow into the R-reservoir by exchanging two bath temperatures is asymmetric under the external field driving, i.e., such thermal asymmetric behavior becomes vanishing as $\Omega = 0$ and $\gamma_{\rm L,1} = \gamma_{\rm R,1}$, shown in Eq. (12). Generally speaking, the external driving could be considered as one additional bosonic terminal [i.e., injecting (extracting) the energy into (out of) the system], which makes the NE-DSBM an effective three-terminal spin setup.

Here, we approximately characterize the asymmetric behavior of the current into the Rth reservoir by the factor [57]

$$R_J = |J_+ + J_-|/\max\{|J_+|, |J_-|\}, \tag{13}$$

where J_+ is identical with $J_{\rm ss}$, and J_- is the current into the right reservoir by exchanging $T_{\rm L}$ and $T_{\rm R}$ of two reservoirs. It is known that based on the standard two-terminal setup in the absence of external driving, J_+ is exactly the current between the Lth and Rth reservoirs, and there is no thermal diode effect for a symmetric setup. While including the external driving, we cannot explicitly classify the energy flow between two reservoirs purely driven by the temperature bias, due to the coherence. One should note that the *asymmetry* comes from the way to measure the heat current, i.e., defining the current as the one into the Rth reservoir, which is unlike the traditional thermal diode effect.

Then, we study the influences of driving amplitude and temperature bias on the asymmetric factor R_J in Fig. 7. By tuning the driving amplitude, the factor shows a monotonic increase and surpasses the unit with weak driving amplitude [e.g., $\Omega \approx 0.03$ shown by a solid red line in Fig. 7(a)], which characterizes the full blockade of J_-. Then, R_J saturates around 2, which implies $J_+ \approx J_-$. This is mainly contributed by the factor that the driving current component dominates the current, which is nearly independent of the temperature bias. We also show the behavior of R_J by increasing the temperature bias in Fig. 7(b). It is found that R_J is robust with strong driving amplitude, compared to the fast decay of R_J in the weak driving case.

IV. CONCLUSION

We study the quantum energy transport in the nonequilibrium driven quantum system exemplified as the spin-boson model, based on a canonical transformation and full-counting statistics. This analytical approach is valid for a wide variety of spectral functions of the bosonic baths, e.g., super-Ohmic and Lorentz forms, and it can be extended to more complex driven quantum systems, e.g., coupled and collective qubits cases. The nonmonotonic behavior of steady-state flow by tuning the Rabi frequency Ω is exhibited. The steady-state flow is naturally divided into three components: (i) the temperature bias flow $J_{\rm t}$, which is generated by the temperature bias of two bosonic baths; (ii) the driving flow $J_{\rm d}$, which is proportional to the square of the driving amplitude; and (iii) the coherence flow $J_{\rm c}$, which mainly stems from the contribution of steady-state off-diagonal density matrix elements. The analytical expressions are exhibited in Eqs. (11a)–(11c). Then, the cooperative effects of the temperature bias and the coherent external driving on the steady-state flow and its components are dissected. The heat flow becomes asymmetric by exchanging two bath temperatures when we tune on the driving amplitude. Moreover, the results show that with an increase of the driving amplitude, the main contribution to steady-state flow changes from $J_{\rm t}$ to the positive driving flow $J_{\rm d}$. The negative coherence flow $J_{\rm c}$ denotes an interference effect of driving and dissipation, and it may not be naively ignored at the strong driving regime. These results may deepen the understanding of nonequilibrium energy transport under an external field driving in quantum transport and quantum thermodynamics. Moreover, it may provide theoretical guidance for the smart control of energy and information in low-dimensional quantum nanodevices.

ACKNOWLEDGMENTS

X.C. acknowledges support from the Fujian Province Natural Science Foundation under Grant No. 2022J01008. We also acknowledge financial support from the NSFC of China (Grants No. 12075199, No. 11704093, No. 11535011, and No. 11874170).

APPENDIX A: DERIVATION OF THE EQUATION OF MOTION OF THE DENSITY MATRIX

This Appendix provides the derivation of the equation of motion of the density matrix in the interaction picture of Eq. (6) with $H_S' = \Omega(s_+ + s_-)/2$, $H_B' = \sum_{k,\nu}(\omega_{k,\nu} - \omega_{\rm d})a_{k,\nu}^\dagger a_{k,\nu}$, and $H_I' = \sum_k \tilde{g}_{k,\rm R}(a_{k,\rm R}^\dagger s_- e^{\frac{i\chi\omega_{k,\rm R}}{2}} + a_{k,\rm R} s_+ e^{-\frac{i\chi\omega_{k,\rm R}}{2}}) + \sum_k \tilde{g}_{k,\rm L}(a_{k,\rm L}^\dagger s_- + a_{k,\rm L} s_+)$. The density matrix of the total system in the interaction picture $\rho_{SB}'^I(\chi,t) = \exp[i(H_S' + H_B')t]\rho_{SB}'(\chi,t)\exp[-i(H_S' + H_B')t]$ yields the equation of motion

$$d\rho_{SB}'^I(\chi,t)/dt = -i\big[V_I'(\chi,t), \rho_{SB}'^I(\chi,t)\big]_\chi, \tag{A1}$$

with the time-dependent interaction Hamiltonian $V_I'(\chi,t) = \exp[i(H_S' + H_B')t]H_I'\exp[-i(H_S' + H_B')t]$, which is

specified as

$$V_I'(\chi,t)=\sum_k\Big(\tilde{g}_{k,\mathrm{R}}a_{k,\mathrm{R}}^\dagger e^{[\frac{i\chi\omega_{k,\mathrm{R}}}{2}+i(\omega_{k,\mathrm{R}}-\omega_\mathrm{d})t]}e^{iH_S't}s_-e^{-iH_S't}+\tilde{g}_{k,\mathrm{L}}a_{k,\mathrm{L}}^\dagger e^{[i(\omega_{k,\mathrm{L}}-\omega_\mathrm{d})t]}e^{iH_S't}s_-e^{-iH_S't}\Big)+\mathrm{H.c.}$$

Under the Born-Markov approximation, the density matrix $\rho_{SB}'^I(\chi,t)$ can be approximated as the product state $\rho_{SB}'^I(\chi,t)=\rho_S'^I(\chi,t)\otimes\rho_B(0)$. And the equation of motion is given by

$$\frac{d}{dt}\rho_{SB}'^I(\chi,t)=-\int_0^t dt'\mathrm{Tr}_B\{[V_I'(\chi,t'),[V_I'\times(\chi,t'),\rho_S'^I(\chi,t)\otimes\rho_B(0)]_\chi]_\chi\},\quad\text{(A2)}$$

where $\rho_S'^I(\chi,t)=\mathrm{Tr}_B[\rho_{SB}'^I(\chi,t)]$. Assuming the two boson baths are in thermal equilibrium, they follow the Bose-Einstein distribution that $\mathrm{Tr}_B(a_{k,\nu}^\dagger a_{k,\nu}\rho_B)=n_\nu(\omega_{k,\nu})$ and $\mathrm{Tr}_B(a_{k,\nu}a_{k,\nu}^\dagger\rho_B)=n_\nu(\omega_{k,\nu})+1$, where $n_\nu(\omega_{k,\nu})$ is the thermal average boson number at mode k given by $n_\nu(\omega_{k,\nu})=[\exp(\omega_{k,\nu}/k_BT_\nu)-1]^{-1}$. Returning to the Schrödinger picture, the equation of motion of the density matrix is given by

$$\frac{d}{dt}\rho_S'(\chi,t)=-i[H_{0s}',\rho_S'(t)]_\chi-\int_0^t\mathrm{Tr}_B[V'(\chi,t)\exp(iH_S'(-t)),\times[\exp(iH_S't')V'(\chi,t')\exp(-iH_S't'),\times\exp(iH_S't)\rho_S'(\chi,t)\otimes\rho_B(0)]_\chi]_\chi dt'.\quad\text{(A3)}$$

where the simplified interaction Hamiltonian is given by

$$V'(\chi,t)=\Big(\sum_k\tilde{g}_{k,\mathrm{R}}a_{k,\mathrm{R}}^\dagger\exp\Big[\frac{i\chi\omega_{k,\mathrm{R}}}{2}+i(\omega_{k,\mathrm{R}}-\omega_\mathrm{d})t\Big]s_-+\sum_k\tilde{g}_{k,\mathrm{L}}a_{k,\mathrm{L}}^\dagger s_-\exp[i(\omega_{k,\mathrm{L}}-\omega_\mathrm{d})t]\Big)+\mathrm{H.c.}$$

APPENDIX B: SOLUTION OF THE MASTER EQUATION WITH FULL COUNTING STATISTICS

This Appendix gives the solution process of the master equation with the superoperator $\hat{\mathcal{L}}(\chi)$. Considering the symmetry of the superoperator, we apply a rotating to the equation of motion,

$$U=\begin{pmatrix}1&0&0&-1\\0&-1&1&0\\0&1&1&0\\1&0&0&1\end{pmatrix}.\quad\text{(B1)}$$

Therefore, the transformed density matrix becomes

$$|\rho_S''(\chi,t)\rangle=|\rho_{11}''(\chi,t),\rho_{12}''(\chi,t),\rho_{21}''(\chi,t),\rho_{22}''(\chi,t)\rangle,\quad\text{(B2)}$$

with $\rho_{11}''(\chi,t)=\rho_{11}'(\chi,t)-\rho_{22}'(\chi,t)$, $\rho_{12}''(\chi,t)=\rho_{21}'(\chi,t)-\rho_{12}'(\chi,t)$, $\rho_{21}''(\chi,t)=\rho_{21}'(\chi,t)+\rho_{12}'(\chi,t)$, and $\rho_{22}''(\chi,t)=\rho_{11}'(\chi,t)+\rho_{22}'(\chi,t)$. The equations of motion are rearranged as

$$\frac{d}{dt}|\rho_S''(\chi,t)\rangle=\hat{\mathcal{L}}'(\chi)|\rho_S''(\chi,t)\rangle,\quad\text{(B3)}$$

with the regrouped superoperator $\hat{\mathcal{L}}'(\chi)$. It is composed of three parts, $\hat{\mathcal{L}}'(\chi)=\hat{\mathcal{L}}_\mathcal{D}'+\hat{\mathcal{L}}_\mathrm{L}'+\hat{\mathcal{L}}_\mathrm{R}'(\chi)$, with the first part of the driving $\hat{\mathcal{L}}_\mathcal{D}'$,

$$\hat{\mathcal{L}}_\mathcal{D}'=\begin{pmatrix}0&-i\Omega&0&0\\-i\Omega&0&0&0\\0&0&0&0\\0&0&0&0\end{pmatrix},\quad\text{(B4)}$$

the second part of the left bath $\hat{\mathcal{L}}_\mathrm{L}'$,

$$\hat{\mathcal{L}}_\mathrm{L}'=\begin{pmatrix}\mathrm{l}_{11}&0&\mathrm{l}_{13}&\mathrm{l}_{14}\\0&\mathrm{l}_{22}&0&0\\0&0&\mathrm{l}_{33}&\mathrm{l}_{34}\\0&0&0&0\end{pmatrix},\quad\text{(B5)}$$

$$\mathrm{l}_{11}=-\tfrac{1}{2}(2\Gamma_{\mathrm{L}1}+\Gamma_{\mathrm{L}2}+\Gamma_{\mathrm{L}3}),\quad\text{(B6a)}$$

$$\mathrm{l}_{13}=\tfrac{1}{2}(\Gamma_{\mathrm{L}2}-\Gamma_{\mathrm{L}3}),\quad\text{(B6b)}$$

$$\mathrm{l}_{14}=-\tfrac{1}{2}(2\gamma_{\mathrm{L}1}+\gamma_{\mathrm{L}2}+\gamma_{\mathrm{L}3}),\quad\text{(B6c)}$$

$$\mathrm{l}_{22}=-\Gamma_{\mathrm{L}1},\quad\text{(B6d)}$$

$$\mathrm{l}_{33}=-\tfrac{1}{2}(\Gamma_{\mathrm{L}2}+\Gamma_{\mathrm{L}3}),\quad\text{(B6e)}$$

$$\mathrm{l}_{34}=\tfrac{1}{2}(2\Gamma_{\mathrm{L}1}+\Gamma_{\mathrm{L}2}+\Gamma_{\mathrm{L}3}),\quad\text{(B6f)}$$

with $\Gamma_{\mathrm{L}j}=[1+2n_L(\omega_\mathrm{j})]\gamma_L(\omega_\mathrm{j})$, and the frequencies ω_j with $\mathrm{j}=1,2,3$ are, respectively, $\omega_1=\eta\,\Delta$, $\omega_2=(\eta\,\Delta-\Omega)$, and $\omega_3=(\eta\,\Delta+\Omega)$, which are concerned with the Mollow triplet. The variables $\gamma_{L\mathrm{j}}$ are determined by the spectral function of the bath,

$$\gamma_{\nu\mathrm{j}}=\gamma_\nu(\omega_j)=\pi\sum_k\tilde{g}_k^2\quad\text{(B7)}$$

$$=\pi\sum_k\left(\frac{\eta\,\Delta g_{k,\nu}}{\eta\,\Delta+\omega_k}\right)^2\delta(\omega_k-\omega)\quad\text{(B8)}$$

$$=\pi\left(\frac{\eta_\nu\,\Delta}{\eta_\nu\,\Delta+\omega}\right)^2J_\nu(\omega_j),$$

with $\nu=(\mathrm{R},\mathrm{L})$ and $j=(1,2,3)$. And $\gamma_{\nu\mathrm{j}}$ is obviously independent of temperature and is the zero-temperature decay rate. The finite-temperature decay factor

$$\Gamma_{\nu\mathrm{j}}=(1+2\mathrm{n}_{\nu\mathrm{j}})\gamma_{\nu,\mathrm{j}},\quad\text{(B9)}$$

with $\mathrm{n}_{\nu\mathrm{j}}=n_\nu(\omega_\mathrm{j})=[\exp(\omega_j/k_BT_\nu)-1]^{-1}$. In the case of zero temperature, $\Gamma_{\mathrm{L}j}=\gamma_{\mathrm{L}j}$. In this paper, we assume the coupling spectra of the left and right bath are the same, $G_\mathrm{L}(\omega)=G_\mathrm{R}(\omega)$, but the temperature of the left and right bath can be controlled independently.

The Lindblad superoperator of the right-bath part $\hat{\mathcal{L}}_\mathrm{R}'(\chi)$ is

$$\hat{\mathcal{L}}_\mathrm{R}'(\chi)=\begin{pmatrix}\mathrm{r}_{11}&0&\mathrm{r}_{13}&\mathrm{r}_{14}\\0&\mathrm{r}_{22}&0&0\\\mathrm{r}_{31}&0&\mathrm{r}_{33}&\mathrm{r}_{34}\\\mathrm{r}_{41}&0&\mathrm{r}_{43}&\mathrm{r}_{44}\end{pmatrix}.\quad\text{(B10)}$$

Because the auxiliary counting projector χ is applied to the right bath, only the Lindblad operator $\hat{\mathcal{L}}'_{\rm R}(\chi)$ is χ-dependent. Then, the matrix elements of the regrouped superoperator of the right bath are

$$\mathrm{r}_{11} = -\tfrac{1}{4}(2\Gamma_{\rm R11} + \Gamma_{\rm R12} + \Gamma_{\rm R13}), \tag{B11a}$$

$$\mathrm{r}_{13} = \tfrac{1}{4}(\Gamma_{\rm R12} - \Gamma_{\rm R13}), \tag{B11b}$$

$$\mathrm{r}_{14} = -\tfrac{1}{4}(2\Gamma_{\rm R21} + \Gamma_{\rm R22} + \Gamma_{\rm R23}), \tag{B11c}$$

$$\mathrm{r}_{22} = \tfrac{1}{4}(-2\Gamma_{\rm R11} + \Gamma_{\rm R32} + \Gamma_{\rm R33}), \tag{B11d}$$

$$\mathrm{r}_{31} = \tfrac{1}{4}(\Gamma_{\rm R32} - \Gamma_{\rm R33}), \tag{B11e}$$

$$\mathrm{r}_{33} = \tfrac{1}{4}(2\Gamma_{\rm R31} - \Gamma_{\rm R32} - \Gamma_{\rm R33}), \tag{B11f}$$

$$\mathrm{r}_{34} = \tfrac{1}{4}(\Gamma_{\rm R22} - \Gamma_{\rm R23}), \tag{B11g}$$

$$\mathrm{r}_{41} = \tfrac{1}{4}(2\Gamma_{\rm R41} + \Gamma_{\rm R42} + \Gamma_{\rm R43}), \tag{B11h}$$

$$\mathrm{r}_{43} = \tfrac{1}{4}(\Gamma_{\rm R43} - \Gamma_{\rm R42}), \tag{B11i}$$

$$\mathrm{r}_{44} = \tfrac{1}{4}(2\Gamma_{\rm R31} + \Gamma_{\rm R32} + \Gamma_{\rm R33}). \tag{B11j}$$

Here, there are four combinations of the three physical quantities $\chi_{\pm}(\omega_{\rm j})$, $n_{\rm R}(\omega_{\rm j})$, and $\gamma_{\rm R}(\omega_j)$:

$$\begin{aligned}\Gamma_{\rm R1j} = \{&[1 + n_R(\omega_{\rm j})][\chi_1(\omega_{\rm j}) + 1] \\ &+ n_R(\omega_{\rm j})[\chi_2(\omega_{\rm j}) + 1]\}\gamma_R(\omega_{\rm j}),\end{aligned} \tag{B12a}$$

$$\begin{aligned}\Gamma_{\rm R2j} = \{&[1 + n_R(\omega_{\rm j})][\chi_1(\omega_{\rm j}) + 1] \\ &- n_R(\omega_{\rm j})[\chi_2(\omega_{\rm j}) + 1]\}\gamma_R(\omega_{\rm j}),\end{aligned} \tag{B12b}$$

$$\begin{aligned}\Gamma_{\rm R3j} = \{&[1 + n_R(\omega_{\rm j})][\chi_1(\omega_{\rm j}) - 1] \\ &+ n_R(\omega_{\rm j})[\chi_2(\omega_{\rm j}) - 1]\}\gamma_R(\omega_{\rm j}),\end{aligned} \tag{B12c}$$

$$\begin{aligned}\Gamma_{\rm R4j} = \{&[1 + n_R(\omega_{\rm j})][\chi_1(\omega_{\rm j}) - 1] \\ &- n_R(\omega_{\rm j})[\chi_2(\omega_{\rm j}) - 1]\}\gamma_R(\omega_{\rm j}),\end{aligned} \tag{B12d}$$

and the functions related to counting operators are defined as $\chi_+(\omega_{\rm j}) = \exp(i\chi\omega_{\rm j})$ and $\chi_-(\omega_{\rm j}) = \exp(-i\chi\omega_{\rm j})$. In above expression, if we let the counting parameter $\chi = 0$, then the function of counting parameter, $\chi_{\pm}(\omega_{\rm j}) = 1$, and the right-bath operator is the same as that of the left bath.

APPENDIX C: DERIVATION OF STEADY-STATE FLOW

This Appendix gives the derivation of steady-state flow. The steady-state cumulant-generating function is derived as

$$\begin{aligned}J_{\rm ss} &= \frac{\partial}{\partial(i\chi)}\left(\lim_{t\to\infty}\frac{\ln \mathcal{Z}_\chi(t)}{t}\right)\Big|_{\chi=0} \\ &= \lim_{t\to\infty}\frac{1}{t}\frac{\partial \ln \mathcal{Z}_\chi(t)}{\partial(i\chi)}\Big|_{\chi=0} \\ &= \langle I|\lim_{t\to\infty}\frac{1}{t}\frac{\partial\hat{\mathcal{L}}'(\chi)t}{\partial(i\chi)}\exp[\hat{\mathcal{L}}'(\chi)t]|\rho''_S(\chi,0)\rangle|_{\chi=0}.\end{aligned} \tag{C1}$$

Then the steady-state solution of energy flow is simplified to

$$J_{\rm ss} = \langle I|\frac{\partial\hat{\mathcal{L}}'(\chi)}{\partial(i\chi)}\Big|_{\chi=0}|\rho''_S(t)\rangle_{\rm ss}, \tag{C2}$$

with the operator solution $|\rho''_S(t)\rangle_{\rm ss} = \lim_{t\to\infty}\exp[\hat{\mathcal{L}}'(\chi)t]|\rho''_S(\chi,0)\rangle|_{\chi=0}$, which is the steady-state of the density matrix $|\rho''_S(\chi,t)\rangle$. Then, the steady-state energy flow is written as

$$\begin{aligned}J_{\rm ss} = &\frac{\partial \mathrm{L}_{41}(\chi)}{\partial(i\chi)}\Big|_{\chi=0}(\rho'_{11} - \rho'_{22})_{\rm ss} \\ &+ \frac{\partial \mathrm{L}_{43}(\chi)}{\partial(i\chi)}\Big|_{\chi=0}(\rho'_{21} + \rho'_{12})_{\rm ss} \\ &+ \frac{\partial \mathrm{L}_{44}(\chi)}{\partial(i\chi)}\Big|_{\chi=0}.\end{aligned} \tag{C3}$$

Compared with Eq. (8), steady-state flow is the particular solution of the transient flow as time approaches infinity, and it is related with the dynamics of the steady state, $(\rho'_{11} - \rho'_{22})_{\rm ss}$ and $(\rho'_{12} + \rho'_{21})_{\rm ss}$.

In the resonant case, $\omega_{\rm d} = \eta\,\Delta$, the steady-state dynamics is solved analytically in Eqs. (10a) and (10b) with the parameters $\gamma_- = \gamma_{\rm R2} - \gamma_{\rm R3} + \gamma_{\rm L2} - \gamma_{\rm L3}$, $\Gamma_- = \Gamma_{\rm R2} - \Gamma_{\rm R3} + \Gamma_{\rm L2} - \Gamma_{\rm L3}$, $\Gamma_1 = \Gamma_{\rm R1} + \Gamma_{\rm L1}$, $\Gamma_+ = \Gamma_{\rm R2} + \Gamma_{\rm R3} + \Gamma_{\rm L2} + \Gamma_{\rm L3}$, $\Gamma = 2\Gamma_{\rm R1} + \Gamma_{\rm R2} + \Gamma_{\rm R3} + 2\Gamma_{\rm L1} + \Gamma_{\rm L2} + \Gamma_{\rm L3}$, $\gamma = 2\gamma_{\rm R1} + \gamma_{\rm R2} + \gamma_{\rm R3} + 2\gamma_{\rm L1} + \gamma_{\rm L2} + \gamma_{\rm L3}$. The zero-temperature decay factor $\gamma_{\nu,\rm j}$ and the finite-temperature decay factor $\Gamma_{\nu\rm j} = (1 + 2\mathrm{n}_{\nu,\rm j})\gamma_{\nu,\rm j}$ are given in Eqs. (B7) and (B9). The driving amplitude Ω splits the driving frequency $\omega_{\rm d} = \eta\,\Delta$ into three frequencies, $\omega_1 = \eta\,\Delta$, $\omega_2 = \eta\,\Delta - \Omega$, $\omega_3 = \eta\,\Delta + \Omega$, which is consistent with the Mollow triplet. From the definition of variables, we see that the two terms, γ_- and Γ_-, depend on the difference of the decay factor of the two side peaks, ω_2 and ω_3. So both terms are entirely generated by the interference of the external driving and the dissipation. Without driving, $\Omega = 0$, the interference factor γ_- is zero, $(\rho'_{12} + \rho'_{21})_{\rm ss} = 0$. Further, the coherence flow disappears.

The derivative of the Liouvillian superoperator is written as

$$\frac{\partial L_{41}(\chi)}{\partial(i\chi)}\Big|_{\chi=0} = \frac{1}{2}\omega_1\Gamma_{\rm R1} + \frac{1}{4}\omega_2\Gamma_{\rm R2} + \frac{1}{4}\omega_3\Gamma_{\rm R3}, \tag{C4a}$$

$$\frac{\partial L_{43}(\chi)}{\partial(i\chi)}\Big|_{\chi=0} = \frac{1}{4}\omega_3\Gamma_{\rm R3} - \frac{1}{4}\omega_2\Gamma_{\rm R2}, \tag{C4b}$$

$$\frac{\partial L_{44}(\chi)}{\partial(i\chi)}\Big|_{\chi=0} = \frac{1}{2}\omega_1\gamma_{\rm R1} + \frac{1}{4}\omega_2\gamma_{\rm R2} + \frac{1}{4}\omega_3\gamma_{\rm R3}. \tag{C4c}$$

Since the counting field is included in the right bath, the derivative of the Liouvillian superoperator $\hat{\mathcal{L}}_\chi$ is only concerned with the parameters in the right bath, which generates an asymmetry about the temperature of the two baths, and it leads to a fundamental difference between the energy transport and the dissipation dynamics, which corresponds with the temperature of both baths. The steady-state flow $J_{\rm ss}$ is naturally divided into three parts, i.e., $J_{\rm ss} = J_{\rm t} + J_{\rm d} + J_{\rm c}$, which

are specified as

$$J_{\mathrm{t}} = \frac{\Gamma_1}{\Gamma\Gamma_1 + 2\Omega^2}\left[\Gamma\left(\frac{1}{2}\omega_1\gamma_{\mathrm{R}1} + \frac{1}{4}\omega_2\gamma_{\mathrm{R}2} + \frac{1}{4}\omega_3\gamma_{\mathrm{R}3}\right) - \gamma\left(\frac{1}{2}\omega_1\Gamma_{\mathrm{R}1} + \frac{1}{4}\omega_2\Gamma_{\mathrm{R}2} + \frac{1}{4}\omega_3\Gamma_{\mathrm{R}3}\right)\right], \tag{C5a}$$

$$J_{\mathrm{d}} = \frac{2\Omega^2}{\Gamma\Gamma_1 + 2\Omega^2}\left(\frac{1}{2}\omega_1\gamma_{\mathrm{R}1} + \frac{1}{4}\omega_2\gamma_{\mathrm{R}2} + \frac{1}{4}\omega_3\gamma_{\mathrm{R}3}\right), \tag{C5b}$$

$$J_{\mathrm{c}} = \frac{\gamma_-}{4\Gamma_+}\left[2\omega_1\Gamma_{\mathrm{R}1}\left(\frac{\Gamma_-\Gamma_1}{\Gamma\Gamma_1 + 2\Omega^2}\right) + \omega_2\Gamma_{\mathrm{R}2}\left(\frac{\Gamma_-\Gamma_1}{\Gamma\Gamma_1 + 2\Omega^2} - 1\right) + \omega_3\Gamma_{\mathrm{R}3}\left(\frac{\Gamma_-\Gamma_1}{\Gamma\Gamma_1 + 2\Omega^2} + 1\right)\right]. \tag{C5c}$$

[1] A. J. Leggett, S. Chakravarty, A. T. Dorsey, M. P. A. Fisher, A. Garg, and W. Zwerger, Rev. Mod. Phys. **59**, 1 (1987).
[2] U. Weiss, *Quantum Dissipative Systems* (World Scientific, Singapore, 1999).
[3] R. Hanson and D. D. Awechalom, Nature (London) **453**, 1043 (2008).
[4] M. Grifoni and P. Hanggi, Phys. Rep. **304**, 229 (1998).
[5] H. P. Breuer and F. Petruccione, *The Theory of Open Quantum Systems* (Oxford University Press, New York, 2006).
[6] M. Hofheinz, H. Wang, M. Ansmann, R. C. Bialczak, E. Lucero, M. Neeley, A. D. O'Connell, D. Sank, J. Wenner, J. M. Martinis, and A. N. Cleland, Nature (London) **459**, 546 (2009).
[7] J. M. Martinis, M. H. Devoret, and J. Clarke, Nat. Phys. **16**, 234 (2020).
[8] X. D. Xu, B. Sun, P. R. Berman, D. G. Steel, A. S. Bracker, D. Gammon, and L. J. Sham, Nat. Phys. **4**, 692 (2008).
[9] J. Gorman, D. G. Hasko, and D. A. Williams, Phys. Rev. Lett. **95**, 090502 (2005).
[10] J. H. Jiang, M. Kulkarni, D. Segal, and Y. Imry, Phys. Rev. B **92**, 045309 (2015).
[11] R. Wang, C. Wang, J. Lu, and J.-H. Jiang, Adv. Phys.: X **7**, 2082317 (2022).
[12] J. Ren, Chin. Phys. Lett. **40**, 090501 (2023).
[13] D. Porras, F. Marquardt, J. von Delft, and J. I. Cirac, Phys. Rev. A **78**, 010101(R) (2008).
[14] A. Lemmer, C. Cormick, D. Tamascelli, T. Schaetz, S. F. Huelga, and M. B. Plenio, New J. Phys. **20**, 073002 (2018).
[15] B. B. Buckley, G. D. Fuchs, L. C. Bassett, and D. D. Awschalom, Science **330**, 1212 (2010).
[16] J. Ren, P. Hanggi, and B. Li, Phys. Rev. Lett. **104**, 170601 (2010).
[17] N. Gupt, S. Bhattacharyya, B. Das, S. Datta, V. Mukherjee, and A. Ghosh, Phys. Rev. E **106**, 024110 (2022).
[18] Z. Wang, L. Q. Wang, J. Z. Chen, C. Wang, and J. Ren, Front. Phys. **17**, 13201 (2022).
[19] K. Schwab, E. A. Henriksen, J. M. Worlock, and M. L. Roukes, Nature (London) **404**, 974 (2000).
[20] L. G. C. Rego and G. Kirczenow, Phys. Rev. Lett. **81**, 232 (1998).
[21] M. Meschke and W. Guichard, and J. P. Pekola, Nature (London) **444**, 187 (2006).
[22] H. Zheng, S. Y. Zhu, and M. S. Zubairy, Phys. Rev. Lett. **101**, 200404 (2008).
[23] Z. H. Li, D. W. Wang, H. Zheng, S. Y. Zhu, and M. S. Zubairy, Phys. Rev. A **80**, 023801 (2009).
[24] Y. Yan, Z. Lu, and H. Zheng, Phys. Rev. A **90**, 053850 (2014).
[25] C. Zhao and H. Zheng, Phys. Rev. A **82**, 043844 (2010).
[26] Z. Lü and H. Zheng, Phys. Rev. A **86**, 023831 (2012).
[27] Z. Lü, Y. Y. Yan, H. S. Goan, and H. Zheng, Phys. Rev. A **93**, 033803 (2016).
[28] Y. Yan, Z. G. Lu, J. Y. Luo, and H. Zheng, Phys. Rev. A **96**, 033802 (2017).
[29] J. F. Huang, J. Q. Liao, L. Tian, and L. M. Kuang, Phys. Rev. A **96**, 043849 (2017).
[30] Z. Ficek, Front. Phys. China **5**, 26 (2010).
[31] Z. Ficek and R. Tanas, Phys. Rep. **372**, 369 (2002).
[32] J. Jing, Z. G. Lu, and Z. Ficek, Phys. Rev. A **79**, 044305 (2009).
[33] C. Guo, A. Weichselbaum, S. Kehrein, T. Xiang, and J. von Delft, Phys. Rev. B **79**, 115137 (2009).
[34] H. Shapourian, Phys. Rev. A **93**, 032119 (2016).
[35] M. M. Sahrapour and N. Makri, J. Chem. Phys. **138**, 114109 (2013).
[36] P. P. Orth, A. Imambekov, and K. Le Hur, Phys. Rev. B **87**, 014305 (2013).
[37] G. M. G. McCaul, C. D. Lorenz, and L. Kantorovich, Phys. Rev. B **97**, 224310 (2018).
[38] J. T. Stockburger and H. Grabert, Phys. Rev. Lett. **88**, 170407 (2002).
[39] Y. Tanimura, J. Phys. Soc. Jpn. **75**, 082001 (2006).
[40] L. Magazzu, S. Denisov, and P. Hanggi, Phys. Rev. E **98**, 022111 (2018).
[41] G. Engelhardt, G. Platero, and J. Cao, Phys. Rev. Lett. **123**, 120602 (2019).
[42] G. Engelhardt and J. Cao, Phys. Rev. Lett. **126**, 090601 (2021).
[43] L. Nicolin and D. Segal, Phys. Rev. B **84**, 161414(R) (2011).
[44] T. Chen, X. B. Wang, and J. Ren, Phys. Rev. B **87**, 144303 (2013).
[45] M. Carrega, P. Solinas, M. Sassetti, and U. Weiss, Phys. Rev. Lett. **116**, 240403 (2016).
[46] C. Wang, J. Ren, and J. S. Cao, Sci. Rep. **5**, 11787 (2015).
[47] C. Wang, J. Ren, and J. S. Cao, Phys. Rev. A **95**, 023610 (2017).
[48] X. Cao, C. Wang, H. Zheng, and D. He, Phys. Rev. B **103**, 075407 (2021).
[49] Z. K. Huang and Y. Zhao, Phys. Rev. A **97**, 013803 (2018).
[50] M. Esposito, U. Harbola, and S. Mukamel, Rev. Mod. Phys. **81**, 1665 (2009).
[51] E. Aurell, R. Kawai, and K. Goyal, J. Phys. A **53**, 275303 (2020).

[52] H. Zheng, Eur. Phys. J. B **38**, 559 (2004).
[53] X. Cao and H. Zheng, Phys. Rev. A **77**, 022320 (2008).
[54] B. R. Mollow, Phys. Rev. **188**, 1969 (1969).
[55] D. Segal, Phys. Rev. B **73**, 205415 (2006).
[56] R. Schmidt, A. Negretti, J. Ankerhold, T. Calarco, and J. T. Stockburger, Phys. Rev. Lett. **107**, 130404 (2011).
[57] L. F. Zhang, J. S. Wang, and B. W. Li, Phys. Rev. B **81**, 100301(R) (2010).